Available online at www.sciencedirect.com

ScienceDirect

Procedia Structural Integrity 11 (2018) 218–225

Structural Integrity Procedia

www.elsevier.com/locate/procedia

XIV International Conference on Building Pathology and Constructions Repair – CINPAR 2018

Nonlinear modelling of the in-plane-out-of-plane interaction in the seismic analysis of masonry infills in r.c. framed buildings

Fabio Mazza[a,]*, Angelo Donnici[a]

[a]*Department of Civil Engineering, Università della Calabria, 87036 Rende (Cosenza), Italy*

Abstract

A five-element macro-model, with four diagonal out-of-plane (OP) nonlinear beams and one horizontal in-plane (IP) nonlinear truss, takes into account the OP and IP failure modes occurring, in the event of seismic loading, for masonry infills (MIs) inserted in reinforced concrete (r.c.) framed buildings. Pivot hysteretic models predict the nonlinear IP and OP force-displacement laws of the infill panel, based on geometrical rules defining loading and unloading branches. Firstly, a calibration of the proposed IP-OP interaction model of MIs is carried out considering full-scale experimental results of traditional masonry typologies. To evaluate the interaction, the numerical results of simultaneous IP and OP cyclic tests on MIs at the top, intermediate and lowest levels of an existing six-storey r.c. framed building are presented, assuming different displacement histories: i) OP loading faster than IP, at the sixth storey; ii) equal IP and OP loading, at the third storey; iii) IP loading faster than OP, at the first storey.

Copyright © 2018 Elsevier B.V. All rights reserved.
Peer-review under responsibility of the CINPAR 2018 organizers

Keywords: masonry infills; in-plane and out-of-plane nonlinear behaviour; in-plane-out-of-plane interaction; infilled r.c. framed buildings; seismic analysis.

1. Introduction

The out-of-plane (OP) behaviour of masonry infills (MIs), inserted in reinforced concrete (r.c.) framed buildings, is recognized as one of the most important failure modes of this non-structural element during an earthquake, which may be a consequence of simultaneous or prior in-plane (IP) damage (Hak et al. 2012). The IP drift ratio is generally reduced at the upper storeys of buildings where, simultaneously, the OP drift ratio increases due to increase of

* Corresponding author. Tel.: +39-0984-496908; fax: +39-0984-494045.
E-mail address: fabio.mazza@unical.it

2452-3216 Copyright © 2018 Elsevier B.V. All rights reserved.
Peer-review under responsibility of the CINPAR 2018 organizers
10.1016/j.prostr.2018.11.029

seismic acceleration, thereby inducing IP-OP interaction with the IP and OP drift ratio limits depending on the corresponding OP and IP demands. Furthermore, field evidence highlights the fact that significant OP damage may also happen at the lower storeys where the highest values of IP drift ratio are attained. Many experimental studies have been conducted in order to characterize the OP behaviour of MIs, but only recently has the correlation between the IP and OP nonlinear responses been analysed (Di Trapani et al. 2018).

The key features of the IP inelastic response of MIs can be obtained by replacing the infill panel with an equivalent diagonal strut (Stafford Smith 1962), without tension, or multiple struts (Al-Chaar 2002) or diagonal strut placed in an eccentric manner (Crisafulli 1997), with the aim of capturing the interaction between the infill panel and the frame. To include the two-way OP arching action also considering the IP-OP interaction, a three-dimensional macro-model of MIs has been proposed, consisting of eight compression-only nonlinear struts connected with a tension-only elastic-linear tie to account for the arching action (Hashemi and Mosalam 2007). Given numerical problems of this approach, two macro-models have recently been proposed (Furtado et al. 2016; Ricci et al. 2018). Among the micro-models, a fibre-section interaction in tension and compression is implemented by Kadysiewski and Mosalam (2009) while a more practical version has been employed by Mosalam and Gunay (2015). Alternatively, two micro-models are available to improve the accuracy of the force transmission to the surrounding frame along both diagonal directions (Oliaee and Magenes 2016; Di Trapani et al. 2018).

Although nonlinear fibre-section models are a very effective way of describing the IP-OP interaction of MIs they are so expensive as to be practically unviable for analysis of complex multi-storey structures. Thus, the aim of the present work is to implement an upgrade of previous analytical macro-models, which includes nonlinear behaviour of MIs in the OP direction, taking into account the reduction in OP capacity in terms of stiffness and strength also produced by IP seismic damage. Specifically, a simplified five-element model, with an equivalent mass of the infill panel divided between two central nodes, takes into account the IP (i.e. compression at the center, compression at the corners, shear sliding and diagonal tension) and OP (i.e. falling debris) failure modes that can occur in the infill panels when subjected to seismic loading.

2. Nonlinear modelling of masonry infills

2.1. In-plane behaviour

The in-plane (IP) nonlinear behaviour of an MI is represented by a five-element model constituted of four support pin-jointed (diagonal) truss elements with rigid behaviour, with inclination θ with respect to the horizontal direction, and one central (horizontal) truss element representing the hysteretic behaviour in terms of tensile and compressive axial forces (Fig. 1a). The backbone curve of the IP lateral force-interstorey drift ($F^{(IP)}$-$\Delta^{(IP)}$) law considers three linear branches (Fig. 1b), depending on parameters α, β and ξ (Cavaleri and Di Trapani 2014). In detail: the first ascending branch corresponds to the uncracked stage until the point C is reached; the second ascending branch represents the post-cracking phase up to point FC, corresponding to the full development of the cracking; the third descending branch describes the post-peak strength deterioration of the infill up to residual values of strength and displacement (point RS, representing a conventional IP collapse point of the infill panel).

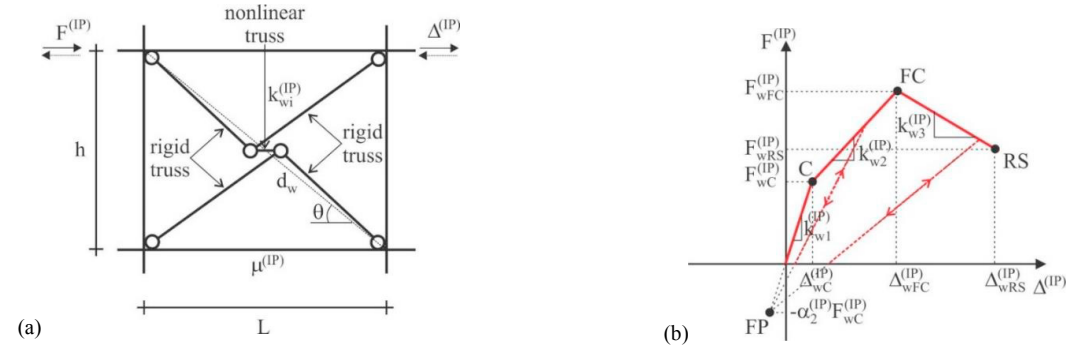

Fig. 1. Nonlinear IP modelling of a masonry infill panel: (a) IP five-element model; (b) IP monotonic and hysteretic (pivot) curves.

Then, the maximum IP lateral strength of the strut is evaluated considering four failure modes (Hak et al. 2012): i.e. diagonal compression, crushing in the corners in contact with the frame, sliding shear along horizontal joints and diagonal tension. Finally, a pivot hysteretic model is adopted to predict the nonlinear force-displacement law of the equivalent diagonal strut (Fig. 1b), based on geometrical rules that define loading and unloading branches corresponding to the asymmetrical tension-compression behaviour of the masonry infills. Further details can be found in Mazza et al. (2018).

2.2. Out-of-plane behaviour

The out-of-plane (OP) nonlinear behaviour of an MI, where L and h are the panel length and height (Fig. 2a), is described by the five-element model without IP interference, considering one support fixed-end rotation (central) beam element, with rigid behaviour, and four diagonal beams representing the OP hysteretic behaviour in terms of shear force and bending moment. Two masses are applied in the two central nodes (i.e. $0.5m^{(OP)}=0.405m_{tot}$, m_{tot} being the total mass of the panel), on the assumption that the OP model has the same fundamental vibration period as the original MI considered simply as a supported vertical beam (Kadysiewski and Mosalam 2009). The backbone curve of the OP transversal force-interstorey drift ($F^{(OP)}$-$\Delta^{(OP)}$) law considers two linear branches (Fig. 2b), but not the initial behaviour of the infill before the formation of an arching action. The initial stiffness of the beam elements with length equal to the infill wall diagonal can be evaluated as

$$k_{w1}^{(OP)} = 48 \cdot E_{eq} \cdot I_{eq} / d_w^3 \tag{1a}$$

where the moment of inertia of the equivalent system

$$I_{eq} = 1.644 \cdot I \cdot \left(d_w / h\right)^3,\ I = L \cdot t_w^3 / 12 \tag{1b}$$

is derived from lumped masses and vibration frequency of the model, while the elasticity modulus

$$E_{eq} = \left(k_p \cdot d_w^3\right) / \left(48 \cdot I_{eq}\right) \tag{1c}$$

is obtained by imposing the equivalence of the stiffness between simply supported bi-diagonal beams and plate (i.e. k_p). Moreover, the OP strength proposed by FEMA 356 (2000) is determined, assuming full contact of the infill panel with the surrounding frame and a slenderness ratio h/t_w of less than or equal to 25

$$q_u = \left(0.7 \cdot f_m' \cdot \lambda_2\right) / \left(h/t_w\right),\ \ \lambda_2 = 1.38 \cdot \left(h/t_w\right)^{-1.41} \tag{2a,b}$$

More specifically, the first ascending branch shown in Fig. 2b represents the cracked stage until the maximum OP resistance of the infill, corresponding to the full arching action (point FAA)

$$F_{wFAA}^{(OP)} = q_u \cdot L \cdot h,\ \ \Delta_{wFAA}^{(OP)} = F_{wFAA}^{(OP)} / k_{w1}^{(OP)} \tag{3a,b}$$

The second softening branch describes the post-peak strength degradation when the arching action appears to be diminishing, both in the horizontal and vertical directions, with significant residual deformations revealing a bulge of the infill and a notable OP slip of the panel (Hak et al. 2014). The residual values of strength and displacement (point RS) represent a conventional OP collapse point of the infill panel

$$F_{wRS}^{(OP)} = \gamma^{(OP)} \cdot F_{wFAA}^{(OP)},\ \ \Delta_{wRS}^{(OP)} = \Delta_{wFAA}^{(OP)} + \xi^{(OP)} \cdot h/2 \tag{4a,b}$$

where $\gamma^{(OP)}$ and $\xi^{(OP)}$ are calibrated as function of the masonry typology (i.e. strong, medium and weak). Finally, the OP residual stiffness is equal to

$$k_{w2}^{(OP)} = tan\left[\left(F_{wFAA}^{(OP)} - F_{wRS}^{(OP)}\right) / \left(\Delta_{wRS}^{(OP)} - \Delta_{wFAA}^{(OP)}\right)\right] \tag{4c}$$

The pivot hysteretic model is adopted to represent OP hysteretic behaviour, being parameter $\alpha_2^{(OP)}$(=0.95) describing a pivot (P) point as function of the full arching action resistance ($F^{(OP)}{}_{wFAA}$).

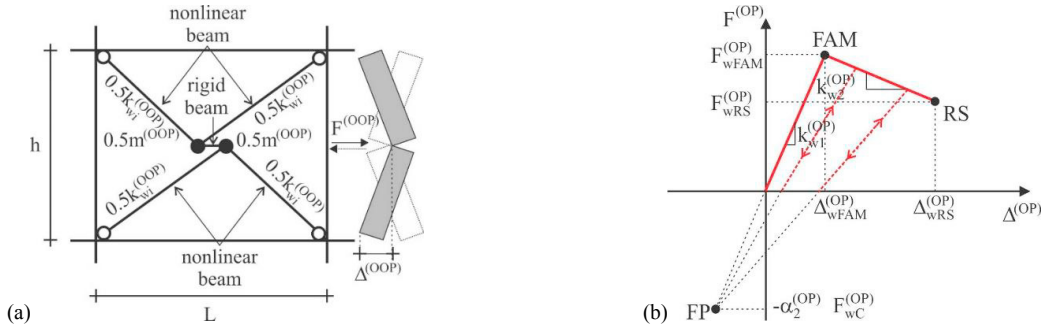

Fig. 2. Nonlinear OP modelling of a masonry infill panel: (a) OP five-element model; (b) OP monotonic and hysteretic (pivot) curves.

2.3. In-plane-out-of-plane interaction modelling

As outlined by many experimental studies, the progression of OP masonry damage is notably influenced by previous IP damage. The IP-OP interaction model proposed in the present work is based on the following fundamental hypotheses: i) IP damage produces a reduction of OP values in strength and stiffness; ii) a bilinear hysteretic law is maintained during the OP damage; iii) OP damage is due to occur as soon as IP drift ratio (i.e. $\Delta^{(IP)}/h$) exceeds the threshold corresponding to the attainment of the maximum IP strength; iv) the effects of OP damage on IP behaviour are not considered. In order to calibrate the relation between maximum values of $\Delta^{(IP)}/h$ and OP decay of strength and stiffness, experimental tests available in the literature are considered with reference to different infill typologies. Firstly, three single-storey single-bay reinforced concrete (r.c.) frame specimens, representing the part of a full-scale r.c. framed structure, are considered, fully infilled with a traditional strong single-leaf unreinforced masonry infill with thickness t_w=35 cm (Hak et al. 2014). The OP cyclic tests have been carried out on the specimens previously damaged in-plane, considering three increasing maximum levels of $\Delta^{(IP)}/h$ (i.e. 1.0%, 1.5% and 2.5%). The following expressions for the percentage reduction factor are obtained for the maximum infill OP strength

$$r_{F,strong}[\%] = \frac{F^{(OP)}_{wFAA,damaged}}{F^{(OP)}_{wFAA,undamaged}} = 69.225 \cdot \left(\frac{\Delta^{(IP)}}{h}\right)^{-0.53} \quad , \quad r_{F,strong}[\%] = \frac{F^{(OP)}_{wFAA,damaged}}{F^{(OP)}_{wFAA,undamaged}} = 42.5 \tag{5a,b}$$

for $(\Delta^{(IP)}/h)$ less (Eq. 5a) or more (Eq. 5b) than 2.5, and initial infill OP stiffness

$$r_{k,strong}[\%] = \frac{k^{(OP)}_{w1,damaged}}{k^{(OP)}_{w1,undamaged}} = 38.369 \cdot \left(\frac{\Delta^{(IP)}}{h}\right)^{-1.382} \quad , \quad r_{k,strong}[\%] = \frac{k^{(OP)}_{w1,damaged}}{k^{(OP)}_{w1,undamaged}} = 10.8 \tag{6a,b}$$

using a regression analysis, on the basis that the OP damage starts once the maximum IP strength is reached (i.e. $(\Delta^{(IP)}/h)_{lower}$=0.5%) while residual mechanical properties persist beyond an upper threshold (i.e. $(\Delta^{(IP)}/h)_{upper}$=2.5%) till the OP collapse point. Moreover, the ultimate values of strength and stiffness are evaluated using Eqs. 4a-4c, where $\gamma^{(OP)}$=0.8 and $\xi^{(OP)}$=0.017 are assumed.

In a similar way, IP-OP tests on weak infill typology, made with hollow clay brick with horizontal holes and thickness t_w=8 cm, have been performed considering three 2/3 scaled single-storey single-bay reinforced concrete (r.c.) frame specimens (Ricci et al. 2017). Preliminary cyclic IP tests were followed by OP monotonic tests, considering: low (0.16%), medium (0.37%) and high (0.58%) levels of $\Delta^{(IP)}/h$. Expressions for the percentage reduction factor of the maximum infill OP strength

$$r_{F,weak}[\%] = \frac{F^{(OP)}_{wFAA,damaged}}{F^{(OP)}_{wFAA,undamaged}} = 17.163 \cdot \left(\frac{\Delta^{(IP)}}{h}\right)^{-0.9617} \quad , \quad r_{F,weak}[\%] = \frac{F^{(OP)}_{wFAA,damaged}}{F^{(OP)}_{wFAA,undamaged}} = 21.25 \tag{7a,b}$$

for $(\Delta^{(IP)}/h)$ less (Eq. 7a) or more (Eq. 7b) than 0.8, and initial infill OP stiffness

$$r_{k,weak}[\%]=\frac{k_{w1,damaged}^{(OP)}}{k_{w1,undamaged}^{(OP)}}=1.962\cdot\left(\frac{\Delta^{(IP)}}{h}\right)^{-2.145},\quad r_{k,weak}[\%]=\frac{k_{w1,damaged}^{(OP)}}{k_{w1,undamaged}^{(OP)}}=3.1 \tag{8a,b}$$

are evaluated for the corresponding entry (i.e. $(\Delta^{(IP)}/h)_{lower}$=0.16%) and final (i.e. $(\Delta^{(IP)}/h)_{upper}$= 0.8%) IP damage thresholds. In the same way as strong infills, ultimate values of strength and stiffness are evaluated with Eqs. 4a-4c, where $\gamma^{(OP)}$=0.6 and $\xi^{(OP)}$=0.016 are assumed. It should be noted that Eqs. 7a-7b and Eqs. 8a-8b are also applied for double-leaf MIs, consisting of two 12 cm thick leaves constituted of horizontally hollowed brick units divided by an intermediate 5 cm cavity, on the assumption that non-contemporaneous OP collapse of masonry panels is avoided. Finally, the mean values of the parameters $\gamma^{(OP)}$ (0.7) and $\xi^{(OP)}$ (0.0165) for both strong and weak typologies are considered by applying Eqs. 4a-4c.

The OP force-displacement law develops on the basis of the IP drift ratio. It is now necessary to define rules on managing the change of curve. It should be noted that OP damage is related to IP response and could occur at any point in the generic OP cycle. Accordingly, specific rules are needed for transition from undamaged to damaged curves and between curves with different levels of damage. These rules change depending on the current branch of the $F^{(OP)}$-$\Delta^{(OP)}$ curve, in line with certain fundamentals: i) the pivot point during unloading from OP damaged curves remains unchanged and referred to the undamaged backbone OP curve; ii) IP-OP interaction does not affect the unloading branch, so degrading effects are not considered in the unloading phase; iii) the damage level reached within the loading phase is moved to the newly damaged curve before proceeding with the next load step.

3. Test structures and loading protocols

A single-storey single-bay r.c. plane frame (Fig. 3a) and a six-storey residential building with r.c. framed structure (Fig. 4) are considered as test structures for the experimental and numerical investigations, respectively. The infill typologies considered in this study represent some of the traditional unreinforced masonry configurations widely used in Europe, consisting of clay bricks in full contact with the surrounding frame members. Loading protocols include two types of displacement-controlled static loading cycles: i) by imposing in-plane cyclic displacements until prescribed drift levels are reached and then testing the infill walls out-of-plane; ii) by involving different combinations of in-plane and out-of-plane cyclic loading simultaneously.

To begin with the first full-scale test structure was designed as part of a four-storey framed building (Hak et al. 2014). Masonry infills consist of traditional unreinforced strong single-leaf infill of 35 cm thickness. Specifically, three fully infilled specimens were subjected to cyclic in-plane tests, at three increasing maximum levels of drift (i.e. $\Delta^{(IP)}/h$=1%, 1.5% and 2.5%), followed by cyclic testing in the out-of-plane direction, until the collapse point. As standard, three cycles were performed at each target displacement. A numerical investigation is also carried out to evaluate IP-OP interaction in relation to decreasing values of strength and stiffness (Hak et al. 2012). To this end, three IP-OP loading histories are examined for each masonry typology, referring to the loading protocols below described with reference to the second test structure. The following typologies of MIs are considered: i) single 30-cm thick leaf (strong); ii) two 12.0-cm thick leaves (medium); single 8cm thin leaf (weak).

Afterwards, a six-storey residential building with r.c. framed structure and symmetric plan, is considered as second test structure (Mazza et al. 2018). Masonry infills are deemed nonstructural elements regularly distributed in the corner bays of the perimeter frames and along the building height. The infill typology selected for this study consists of the same strong single-leaf panel considered for the first test structure. The geometric dimensions of the perimeter frames along the main in-plan Y direction are shown in Fig. 3b, together with the cross section of beams and columns. Numerical tests are carried out at the top, intermediate and lowest levels of the test structure, considering masonry infill of the exterior frames. Specifically, three different loading histories are examined: i) displacement history n.1 (DH1), with OP cyclic loading faster than IP at the sixth storey; ii) displacement history n.2 (DH2), with equal IP and OP cyclic loading at the third storey; iii) displacement history n.3 (DH3), with IP cyclic loading faster than OP at the first storey. Each IP and OP cycle is characterized by a maximum value of displacement higher than in the previous cycle and increasing until preset drift thresholds, high enough to bring the masonry panel to the IP and/or OP collapse point: i.e. $\Delta^{(IP)}_{DH1}$=33 mm and $\Delta^{(OP)}_{DH1}$=49.5 mm, at the sixth storey; $\Delta^{(IP)}_{DH2}$=33 mm and $\Delta^{(OP)}_{DH2}$=33 mm, at the third storey; $\Delta^{(IP)}_{DH3}$=60mm and $\Delta^{(OP)}_{DH3}$=40 mm, at the first storey.

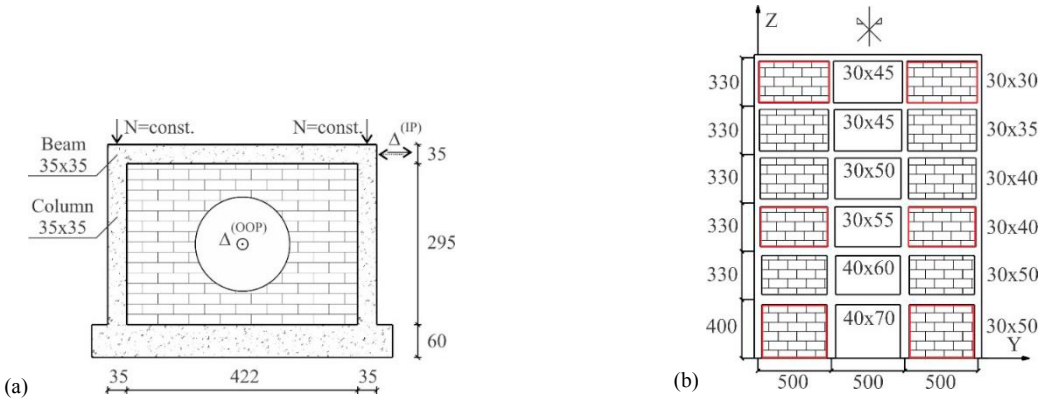

Fig. 3. Test structures for experimental and numerical investigations.

4. Numerical results

The new five-element macro-model proposed in this work for predicting the interaction between in-plane and out-of-plane behaviour of masonry infill is first implemented in a C++ computer code for the nonlinear static (monotonic and cyclic) analysis of r.c. framed structures. To this end, a step-by-step procedure is considered, allowing continuous reproduction of the OP strength and stiffness degradation due to preceding and concurrent IP damage. At each step of the analysis, the algorithm checks the IP drift ratio corresponding to the nonlinear (horizontal) behaviour of the truss element and modifies the OP mechanical properties of the four nonlinear (diagonal) beam elements. As described above, both trilinear IP and bilinear OP backbone curves highlight a softening branch after maximum strength is attained, while the corresponding IP and OP cyclic responses depend on unloading-reloading pivot parameters.

Full-scale experimental tests available in the literature are taken into account to calibrate the numerical model and verify its reliability to reproduce the IP-OP nonlinear interaction, with reference to different masonry typologies and loading histories. To this end, numerical (solid green line) and experimental (solid black line) OP force-displacement curves are plotted in Fig. 4, considering previously damaged specimens constituted of strong MIs. In particular, out-of-plane cyclic tests for strong single-leaf masonry infills have been carried out on the specimens of the first test structure shown in Fig. 3a, previously damaged in-plane with a maximum drift ratio of 1% (Fig. 4a), 1.5% (Fig. 4b) and 2.5% (Fig. 4c) reached via cyclic loading. In all the examined cases, the proposed model provides a reliable assessment of the experimental backbone curves and an acceptable fit with the experimental cyclic response. A significant difference is found between the OP results obtained with different levels of previous IP damage, highlighting a reduction of the initial stiffness and maximum and residual strengths for the highest IP drift ratio. A good approximation of the softening branch is generally obtained for increasing values of the OP drift ratio. It should be noted that unloading and reloading phases occur along the same straight line resulting from the hypotheses of the OP pivot algorithm. It is not possible therefore to capture the internal cycles of the OP experimental laws when three cycles are applied for each peak displacement, in line with the loading protocols of the first test structure. However, such straight lines appropriately reproduce the global panel response, capturing the key values (i.e. minimum and maximum) of the cyclic displacements.

Afterwards, a numerical investigation is carried out in order to obtain relevant information on the OP nonlinear behaviour and degradation mode of the most common masonry configurations used in European building. To this end, IP and OP cyclic tests are simulated, on three main variable parameters: i) typology of MIs; ii) geometric dimensions of the surrounding r.c. frame; iii) histories of the IP and OP displacement. Numerical results in terms of force-displacement (F-Δ) laws are shown in Figs. 5-6, distinguishing: a) cyclic response (black line); b) undamaged OP backbone curves (red lines); c) damaged OP backbone curve at the end of the loading history (blue line). The displacement history provides for a pair of IP and OP synchronous paths with progressively increasing amplitude (i.e. with minimum and maximum values at the same step), assuming that maximum drift (i.e. $\Delta^{(IP)}/h=1\%$ and $\Delta^{(OP)}/(0.5h)=1\%$) is reached after 20 cycles.

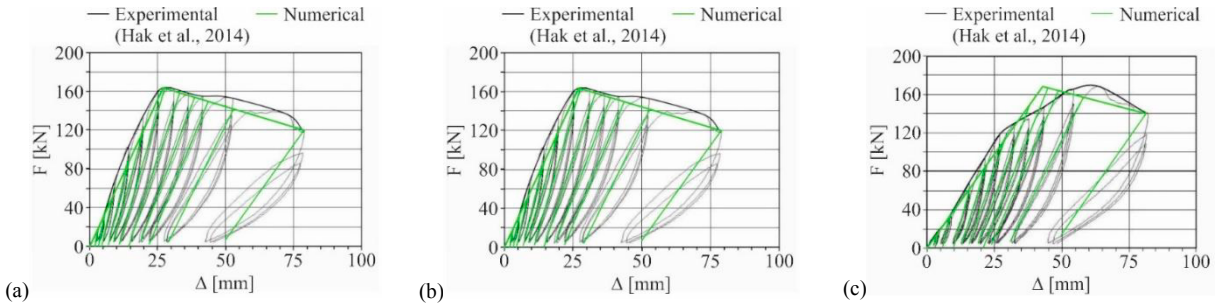

Fig. 4. Comparison between experimental and numerical OP results for strong infill typology:
(a) $\Delta^{(IP)}/h$=1.0%; (b) $\Delta^{(IP)}/h$=1.5%; (c) $\Delta^{(IP)}/h$=2.0%.

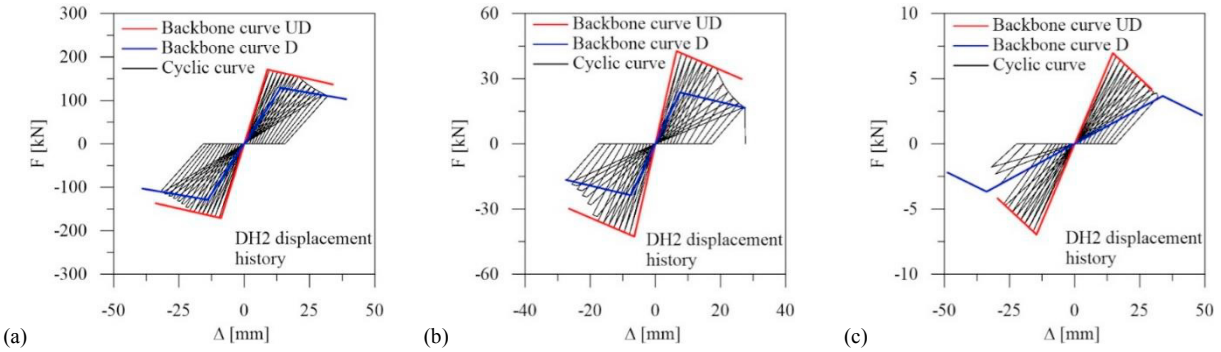

Fig. 5. OP force-displacement laws for different infill typologies and DH2 displacement history:
(a) strong MI; (b) medium MI; (c) weak MI.

As shown, the OP degradation of the strong infill typology starts at roughly the half-way point of the displacement history, reaching the end of the test with a certain leeway safety with regard to the collapse condition (Fig. 5a). The medium infill typology has a lower OP capacity than the strong infill, with OP collapse (Fig. 5b) induced by OP degradation activated during the final cycles of the test. Finally, OP degradation of the backbone curve comes quickly for the weak infill, reaching high displacements after a few steps (Fig. 5c). Similar graphs are reported in Fig. 6 with reference to three MIs of the sixth (Fig. 6a), third (Fig. 6b) and first (Fig. 6c) storey of the test structure shown in Fig. 3b. At each masonry infill a displacement history consistent with its position within the frame is assigned, so as to effectively analyse how much OP degradation occurs along the building height. As shown in Fig. 6a, the IP displacement history at the sixth storey only produces a slight OP degradation. The OP cycles are almost entirely related to the corresponding undamaged (UD) backbone curve. On the other hand, the maximum IP and OP drift ratio of the MI applied at the third storey does not produce collapse (Fig. 6b).

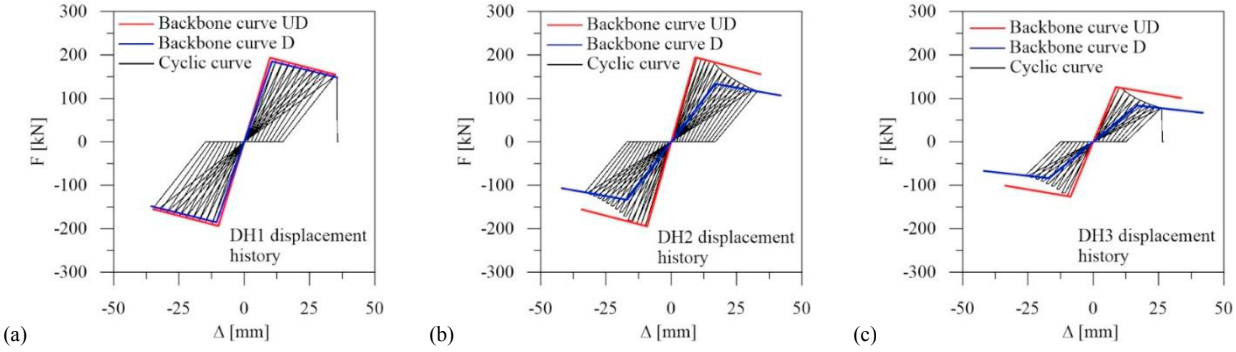

Fig. 6. OP force-displacement laws for strong infill typology and different displacement histories:
(a) sixth level; (b) third level; (c) first level.

A large number of IP cycles exceeds the second branch of the backbone curve, thus triggering a high level of OP degradation. Approximately half of the cyclic loading-unloading process takes place on the undamaged OP curve, then moving to the final damaged one. The IP displacement history considered at the first level results in the IP collapse (Fig. 6c) complemented by a high level of OP degradation. In fact, the transition from undamaged to final damaged curve occurs earlier than in the previous cases because of the faster IP drift ratio.

5. Conclusions

A five-element macro-model comprising four diagonal nonlinear beams and one central nonlinear truss for the prediction of the out-of-plane (OP) and in-plane (IP) behaviour of masonry panels, respectively, is first developed and implemented in a computer code for the nonlinear static (monotonic and cyclic) analysis of r.c. infilled framed structures. Two full-scale experiments carried out on strong and weak masonry infills, where specimens previously damaged in-plane through cyclic tests undergo OP cyclic tests until collapse, are considered to calibrate the proposed model. A reliable assessment of the OP backbone and cyclic curves has been obtained by using the proposed model. Moreover, a numerical investigation has been carried out with reference to strong, medium and weak typologies of masonry infills and three cyclic displacement hystories (i.e. OP loading faster, equal or lower than IP). It should be noted that the strong infill has higher OP capacity than the medium infill, while the OP degradation comes very quickly for the weak infill unlike the strong infill. Finally, masonry panels of the upper storeys (DH1 displacement history) show an OP collapse with little (strong MI) or no (medium and weak MIs) degradation, while a high level of OP degradation is resulted at the lower storeys (DH3 displacement history).

Acknowledgements

This work was financed by M.I.U.R. (Italian Ministry of University and Research) in accordance with the Financing Fund of the Basic Research (year 2018).

References

Al-Chaar, G., 2002. Evaluating strength and stiffness of unreinforced masonry infill structures. Report No. ERDC/CERL-TR-02-1, Engineer Research and Development Center, Construction Engineering Research Laboratory, Champaign, IL, USA.

Cavaleri, L., Di Trapani, F., 2014. Cyclic response of masonry infilled RC frames: Experimental results and simplified modeling. Soil Dynamics and Earthquake Engineering 65, 224-242.

Crisafulli, F.J., 1997. Seismic behaviour of reinforced concrete structures with masonry infills, PhD Thesis, University of Canterbury, Christchurch, New Zealand.

Di Trapani, F., Shing, P.B., Cavaleri, L., 2018. Macroelement model for in-plane and out-of-plane responses of masonry infills in frame structures. Journal of Structural Engineering 144(2), paper 04017198.

FEMA 356, 2000. Prestandard and commentary for the seismic rehabilitation of buildings. Federal Emergency Management Agency, Washington, D.C..

Furtado, A., Rodrigues, H., Arêde, A., Varum, H., 2016. Simplified macro-model for infill masonry walls considering the out-of-plane behaviour. Earthquake Engineering & Structural Dynamics 45, 507-524.

Hak, S., Morandi, P., Magenes, G., Sullivan, T.J., 2012. Damage control for clay masonry infills in the design of rc frame structures. Journal of Earthquake Engineering 16(S1), 1-35.

Hak, S., Morandi, P., Magenes, G., 2014. Out-of-plane experimental response of strong masonry infills. Proceedings of the Second European Conference on Earthquake Engineering and Seismology. Istanbul, Turkey, August 25-29.

Hashemi, A., Mosalam, K.M., 2007. Seismic evaluation of reinforced concrete buildings including effects of masonry infill walls. Pacific Earthquake Engineering Research Center College of Engineering, University of California, Berkeley, PEER Report 2007/100.

Kadysiewski, S., Mosalam, K.M., 2009. Modeling of unreinforced masonry infill walls considering in-plane and out-of-plane interaction. Pacific Earthquake Engineering Research Center College of Engineering, University of California, Berkeley, PEER Report 2008/102.

Mazza, F., Mazza, M., Vulcano, A., 2018. Base-isolation systems for the seismic retrofitting of r.c. framed buildings with soft-storey subjected to near-fault earthquakes. Soil Dynamics and Earthquake Engineering 109, 209-221.

Mosalam, K.M., Gunay, S., 2015. Progressive collapse analysis of RC frames with URM infill walls considering in-plane/ out-of-plane interaction. Earthquake Spectra 31(2), 921-943.

Oliaee, M., Magenes, G., 2016. In-Plane/Out-of-Plane Interaction in the Seismic Response of Masonry Infills in RC Frames. Proceedings of the 16th International Brick and Block Masonry Conference, Padova, Italy, 26-30 June.

Ricci, P., Di Domenico, M., Verderame, G.M., 2018. Empirical-based out-of-plane URM infill wall model accounting for the interaction with in-plane demand. Earthquake Engineering & Structural Dynamics 47(3), 802-827.

Ricci, P., Di Domenico, M., Verderame, G.M., 2017. Experimental assessment of the out-of-plane seismic response of URM infill walls. Proceedings of the XVII National Conference on Earthquake Engineering, ANIDIS, Pistoia, Italy, September 17-21.

Stafford Smith, B., 1962. Lateral stiffness of infilled frames. Journal of Structural Division ASCE 88(6), 183-199.